

JefiPIC: A 3-D Full Electromagnetic Particle-in-Cell Simulator Based on the Jefimenko's Equations on GPU

Jiannan Chen¹, Jun-Jie Zhang^{1,*}, Xueming Li², Yongtao Zhao³

1. Northwest Institute of Nuclear Technology, Xi'an, 710024, China

2. Institute of Applied Physics and Computational Mathematics, Beijing, 100094, China

3. MOE Key Laboratory for Nonequilibrium Synthesis and Modulation of Condensed Matter, School of Science, Xi'an Jiaotong University, Xi'an, 710049, China

* Corresponding to Email: zjacob@mail.ustc.edu.cn

Abstract: In this paper, we have proposed a new 3-D particle-in-cell (PIC) code which employs the Jefimenko's equations as the electromagnetic field solver. The challenging integral task has been made possible with the help of the state-of-the-art graphic processing units (GPU) apparatus. To match the location of the fields and current densities defined in Jefimenko's equations, we have modified the field and charge interpolation methods. Different from the classical finite-difference time-domain (FDTD) method, the integral equations do not require strict charge-conservation field interpolation approaches during the particle emission moments. Our proposed method can naturally deal with the electrostatic problems and does not need to design the elaborate boundary conditions. To verify the code, we compare the particle evolution of a pure electron system simulated by other three codes: EPOCH, UNIPIC, and RGB-Maxwell. The numerical results imply that the combination of the Jefimenko's equations and the PIC method can provide more accurate particle distributions and electromagnetic fields in describing open-boundary plasma systems, especially when the electrostatic/low-frequency electromagnetic fields are dominant. Our verification demonstrates that we can accomplish such task within an acceptable execution time with the use of the GPU.

Keywords: particle-in-cell, finite-difference time-domain, Jefimenko's equation, interpolation method, GPU

1 Introduction

1.1 Background

Particle-in-cell (PIC), a method that adopts the concept of macro-particles to describe the particles in similar phase space states, was first put forward by Dawson for studying the Langmuir wave in 1-D electrostatic plasma in the 1960s [1]. Later, Langdon and Birdsall modified the PIC model to the finite-size particle [2] or particle cloud [3], and solved the problem of the Coulomb collision between particles. Further, Marder [4] and Villasenor [5] amended the error of the electric field divergence, and Birdsall [6] and Vahedi [7] introduced the Monte Carlo collision into PIC, which made PIC step into the practical application. Nowadays, PIC is often used to simulate the controlled/laser thermonuclear fusion [8],[9], study nuclear explosion [10],[11],[12] and space physics effects [13], or design the vacuum electronic devices [14],[15],[16].

The PIC method provides an intuitive description of the motion of charged particles, and it is more accessible for researchers to analyze the data. Under this condition, many mature commercial software and open-source PIC codes have shown up, for example, MAGIC [17], XOOPIIC [18], ICEPIC [19], UNIPIC [20], EPOCH [21],[22] and so on.

On the whole, the PIC model includes two important parts. One is to update the dynamics of electromagnetic (EM) fields from Maxwell's equations,

$$\varepsilon \frac{\partial \mathbf{E}}{\partial t} = \nabla \times \frac{\mathbf{B}}{\mu} - \mathbf{J}, \quad (1)$$

$$\frac{\partial \mathbf{B}}{\partial t} = -\nabla \times \mathbf{E}, \quad (2)$$

$$\nabla \cdot \mathbf{E} = \frac{\rho}{\varepsilon}, \quad (3)$$

$$\nabla \cdot \mathbf{B} = 0, \quad (4)$$

where \mathbf{E} and \mathbf{B} are the electric and magnetic fields, ε and μ are the permittivity and permeability of the medium, ρ and \mathbf{J} are the electric density and electric current density.

The other part is to update and follow the positions and velocities of the charged particles by the Newton–Lorentz force equations of motion

$$\frac{d}{dt} \gamma m \mathbf{v} = q(\mathbf{E} + \mathbf{v} \times \mathbf{B}), \quad (5)$$

$$\frac{d}{dt} \mathbf{r} = \mathbf{v}, \quad (6)$$

where m , q , \mathbf{r} , and \mathbf{v} are the mass, charge, displacement, and velocity of the particle, respectively. The relativistic factor is

$$\gamma = \frac{1}{\sqrt{1 - (v/c)^2}} = \sqrt{1 + (u/c)^2}, \quad (7)$$

where c is the speed of light, $\mathbf{u} = \gamma \mathbf{v}$.

The current continuity equation is satisfied automatically

$$\frac{\partial \rho}{\partial t} + \nabla \cdot \mathbf{J} = 0. \quad (8)$$

As a result, to solve the Maxwell's equations, we can only consider the first two curl equations Eqs. (1) ~ (2). The rest two divergence equations Eqs. (3) ~ (4) can be obtained accordingly. The usual method for solving Eqs. (1) ~ (2) in PIC is the FDTD method [23], which is born naturally to calculate the curl equations due to its sparsity and simplicity compared with other methods, such as the finite element method (FEM) [24],[25] which needs to design complex basic functions. Meanwhile, due to Eq. (8), once an electron is produced, there will generate certain electric fields behaving like positive particles depositing where the electron emits. We name the positive particle after “invented positive charge”, of which charge is different according to different field interpolation methods [26],[27],[28]. Some field interpolation methods make the amount of the “invented positive charge” just reverse to that of the emission electron, which are called the charge-conservation interpolation methods.

1.2 Motivation

The description of plasma systems in terms of the FDTD-based PIC simulation encounters two challenges: it requires elaborate algorithms to cut off the propagation of the EM fields and it is weak at describing electrostatic/low frequency EM fields. Both scenarios can be simplified if one adopts the integral equations such as the Jefimenko's equations [29],[30]. However, known as the general solutions of the Maxwell's equations, Jefimenko's equations are resource-consuming, especially when combined with

the PIC methods.

In this paper, we have proposed a Jefimenko-based PIC method named JefiPIC, which employs the Jefimenko's equations to provide the EM fields in the PIC simulation. The challenging task is made possible on the GPU device. As long as given the initial condition of the charged particles and the background EM fields, our code will automatically compute the space-time distribution of the source terms ρ and \mathbf{J} , as well as the evolution of the plasma. Our method is beneficial in describing the plasma systems with open physical boundaries, such as the space plasma [31], quark gluon plasma [32] or high-altitude nuclear explosion [33],[34], which are not designed to deal with the interaction of fields and the complicated geometrical objects [35]. Meanwhile, our method naturally incorporates the capability in simulating the interactions between low frequency fields and plasmas [15].

In general, JefiPIC has certain advantages over them in some areas:

First, JefiPIC can naturally mimic the evolution of low frequency or electrostatic plasmas. It is reported that the FDTD method encounters difficulties in describing low frequency EM effects [36],[37], hence we usually use the electrostatic Poisson equation [14] as a better option in the PIC simulation, which is more suitable for the stable solution.

Second, one needs to employ proper boundary conditions [38],[39] to cut off and then absorb the EM fields in the FDTD method. The numerical results via the FDTD method are sensitive to the choice of the boundary conditions. Minor errors in the potential reflected waves would raise obvious errors to the whole plasma system. Since we do not need to set the field boundary conditions in JefiPIC, our method is physically and algorithmically simpler in describing open-boundary plasma systems.

Third, when the particles emit, the FDTD-based PIC generates undesired charge conservation errors depending on the field interpolations methods. JefiPIC, on the other hand, does not encounter such numerical difficulties.

Fourthly, the conservation of charge law will also lead to a problem when we simulate a pure electron system in the free space. In such condition, we need to amend the electric field divergence assuming that the initial electrons have already spread their fields to infinity. If the electron emission is continuously carried out during the computation, the amendments should be adopted at each moment a particle emits. In JefiPIC, we do not encounter such challenge as well.

However, the numerical simulation of integral equations, such as Jefimenko's equations, are extremely time consuming, since the integral operation is performed over the entire source volume with retarded time. For a performance enhancement, we use the GPU-based package JefiGPU [40]. JefiGPU performs the Jefimenko's equation directly on GPU with the help of the high dimensional integration package ZMCintegral [41]. With the utilization of JefiGPU, we can perform the evolution of the plasma systems within an acceptable execution time. Meanwhile, we also implement the particle motion equations on GPU, so that the proposed JefiPIC is a fully GPU-based plasma simulator. All quantities are consistently defined on the GPU memory which guarantees a fast execution.

The paper is organized as follows. In Sec. 2 we show the detailed designing process of our proposed JefiPIC method, including the interpolation method of particles and fields and the Jefimenko's equations. In Sec. 3, we compare the results among JefiPIC, UNIPIC, EPOCH and RBG-Maxwell [32],[42] by investigating the evolutions of three different pure electron systems, and analyze the advantages of JefiPIC over the other codes. In Sec. 4, we conclude the work and discuss the future research direction.

2 Method

2.1 Jefimenko's equation

The EM fields in JefiPIC are obtained by the Jefimenko's equations

$$\mathbf{E}(\mathbf{r}, t) = \frac{1}{4\pi\epsilon_0} \int \left[\frac{\mathbf{r} - \mathbf{r}'}{|\mathbf{r} - \mathbf{r}'|^3} \rho(\mathbf{r}', t_r) + \frac{\mathbf{r} - \mathbf{r}'}{|\mathbf{r} - \mathbf{r}'|^2} \frac{1}{c} \frac{\partial \rho(\mathbf{r}', t_r)}{\partial t} - \frac{1}{|\mathbf{r} - \mathbf{r}'|} \frac{1}{c^2} \frac{\partial \mathbf{J}(\mathbf{r}', t_r)}{\partial t} \right] d^3 \mathbf{r}', \quad (9)$$

$$\mathbf{B}(\mathbf{r}, t) = -\frac{1}{4\pi} \int \left[\frac{\mathbf{r} - \mathbf{r}'}{|\mathbf{r} - \mathbf{r}'|^3} \times \mathbf{J}(\mathbf{r}', t_r) + \frac{\mathbf{r} - \mathbf{r}'}{|\mathbf{r} - \mathbf{r}'|^2} \times \frac{1}{c} \frac{\partial \mathbf{J}(\mathbf{r}', t_r)}{\partial t} \right] d^3 \mathbf{r}', \quad (10)$$

$$t_r = t - |\mathbf{r} - \mathbf{r}'|, \quad (11)$$

where t_r is the retarded time, and (\mathbf{r}, t) represents the space-time point. $\mathbf{r} = (x, y, z)$ and $\mathbf{r}' = (x', y', z')$ refer to the displacements in the observation and source region. Given the current density \mathbf{J} and charge density ρ in the space-time, the EM fields at point \mathbf{r} can be calculated via Eqs. (9) ~ (11). Once we obtain the EM fields, the particles are easily pushed according to the Newton–Lorentz functions Eqs. (5) ~ (6).

In JefiPIC, we divide the source region and observation region with the same cuboid grids for numerical computation. Under this condition, Eqs. (9) ~ (11) are discretized as

$$\begin{aligned} \mathbf{E}(\mathbf{r}, t) = & \frac{dx'dy'dz'}{4\pi\epsilon_0} \sum_{i,j,k} \left[\frac{\mathbf{r} - \mathbf{r}'_{i,j,k}}{|\mathbf{r} - \mathbf{r}'_{i,j,k}|^3} \rho(\mathbf{r}'_{i,j,k}, t_r) \right. \\ & + \frac{\mathbf{r} - \mathbf{r}'_{i,j,k}}{|\mathbf{r} - \mathbf{r}'_{i,j,k}|^2} \frac{1}{c} \frac{\rho(\mathbf{r}'_{i,j,k}, t_r) - \rho(\mathbf{r}'_{i,j,k}, t_r - dt)}{dt} \\ & \left. - \frac{1}{|\mathbf{r} - \mathbf{r}'_{i,j,k}|} \frac{1}{c^2} \frac{\mathbf{J}(\mathbf{r}'_{i,j,k}, t_r) - \mathbf{J}(\mathbf{r}'_{i,j,k}, t_r - dt)}{dt} \right] \end{aligned} \quad (12)$$

$$\begin{aligned} \mathbf{B}(\mathbf{r}, t) = & -\frac{dx'dy'dz'}{4\pi} \sum_{i,j,k} \left[\frac{\mathbf{r} - \mathbf{r}'_{i,j,k}}{|\mathbf{r} - \mathbf{r}'_{i,j,k}|^3} \times \mathbf{J}(\mathbf{r}'_{i,j,k}, t_r) \right. \\ & + \frac{\mathbf{r} - \mathbf{r}'_{i,j,k}}{|\mathbf{r} - \mathbf{r}'_{i,j,k}|^2} \times \frac{1}{c} \frac{\mathbf{J}(\mathbf{r}'_{i,j,k}, t_r) - \mathbf{J}(\mathbf{r}'_{i,j,k}, t_r - dt)}{dt} \left. \right] \end{aligned} \quad (13)$$

$$t_r = t - |\mathbf{r} - \mathbf{r}'_{i,j,k}|, \quad (14)$$

where the indices i, j , and k denote the index of the grids in the source region. The numerical value for $\mathbf{r}'_{i,j,k}$ is simply the coordinate at the center of the grid, and dx' , dy' , and dz' are the sizes of the grid in the source region. For computational convenience, \mathbf{J} , ρ , \mathbf{E} and \mathbf{B} are all defined at the center of the grids.

2.2 Particle moving

The Newton–Lorentz force equations are discretized by the central leap-frog difference method as

$$\frac{\gamma m(\mathbf{v}^{n+1/2} - \mathbf{v}^{n-1/2})}{dt} = q \left(\mathbf{E}^n + \frac{\mathbf{v}^{n+1/2} + \mathbf{v}^{n-1/2}}{2} \times \mathbf{B}^n \right), \quad (15)$$

$$\frac{\mathbf{r}^{n+1} - \mathbf{r}^n}{dt} = \mathbf{v}^{n+1/2}, \quad (16)$$

where the superscript n denotes the n^{th} time step in simulation. However, the advancement of velocity is an implicit equation which is difficult to solve directly. So, the Boris particle pusher is employed, and Eq. (15)

is separated into three steps as

$$\mathbf{v}^- = \mathbf{v}^{n-1/2} + \frac{q\mathbf{E}^n}{m} \frac{dt}{2}, \quad (17)$$

$$\frac{(\mathbf{v}^+ + \mathbf{v}^-)}{dt} = \frac{q}{2\gamma m} (\mathbf{v}^+ + \mathbf{v}^-) \times \mathbf{B}^n, \quad (18)$$

$$\mathbf{v}^{n+1/2} = \mathbf{v}^+ + \frac{q\mathbf{E}^n}{m} \frac{dt}{2}. \quad (19)$$

2.3 Charge and field interpolation method

Since the electromagnetic fields, currents, and charge densities need to be allocated at the center of the grids in Jefimenko's equations which is different from that in FDTD, we should modify the field and particle interpolation methods. The traditional PIC methods usually adopt two interpolation methods. One is the so-called charge conservation method, while it will bring numerical noises inevitably. The other is the linear interpolation method with first-order accuracy but less noises. However, the latter one breaks the charge conservation law. In fact, some researchers employ higher accuracy interpolation methods such as Lagrange interpolation or spline interpolation, but the more complex and time-consuming executions limit their applications.

Because of the difference between integral equations and difference equations, JefiPIC does not face the charge conservation problem. Hence, we use the first-order linear interpolation method, which has acceptable numerical noises and computational time.

In the 3-D model, linear interpolation is regarded as the volume-weighted interpolation. For convenience, we use a 2-D model, which utilizes the first-order area-weighted interpolation, to explain how the particle interpolation works in Figure 1. Assuming that there is one particle in some source region, labeled by a “star”, the charge of this particle should be allocated to its nearest center nodes indicated by the solid points. In a 3-D model, one particle should be allocated to 8 nodes, while in a 2-D model there are only 4 nodes with indices (i, j) , $(i+1, j)$, $(i, j+1)$ and $(i+1, j+1)$. According to the area-weighted interpolation method, the allocated charge on one node is equal to the charge of the particle times the weight, which is ratio of the shaded area of its thither corresponding rectangle to the area of one grid.

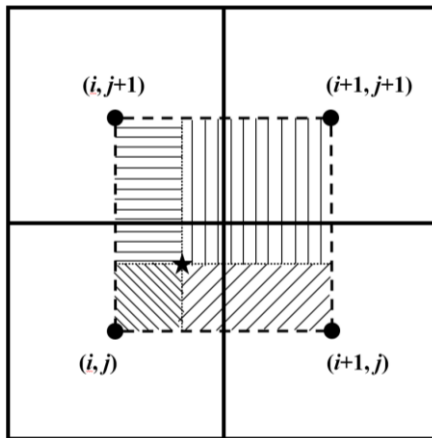


Figure 1. Area-weighted interpolation. The particle is indicated by a “star” and is interpolated to the four neighboring grids according to the ratio of the corresponding shaded area to the grid area.

Since the variables are all defined at the center of the grids, we firstly need to find the indices of the

nodes

$$i = \left[\frac{x - 0.5 \cdot dx'}{dx'} \right], \quad j = \left[\frac{y - 0.5 \cdot dy'}{dy'} \right], \quad k = \left[\frac{z - 0.5 \cdot dz'}{dz'} \right]. \quad (20)$$

where the square brackets mean rounding down. Following the first-order volume-weighted interpolation method, particles with index (i, j, k) should be interpolated to the adjacent grids. Thus, the charge densities on the nearest nodes are expressed as

$$\rho_{i,j,k} = (1 - \alpha)(1 - \beta)(1 - \chi)\rho, \quad (21)$$

$$\rho_{i+1,j,k} = \alpha(1 - \beta)(1 - \chi)\rho, \quad (22)$$

$$\rho_{i,j+1,k} = (1 - \alpha)\beta(1 - \chi)\rho, \quad (23)$$

$$\rho_{i,j,k+1} = (1 - \alpha)(1 - \beta)\chi\rho, \quad (24)$$

$$\rho_{i+1,j+1,k} = \alpha\beta(1 - \chi)\rho, \quad (25)$$

$$\rho_{i+1,j,k+1} = \alpha(1 - \beta)\chi\rho, \quad (26)$$

$$\rho_{i,j+1,k+1} = (1 - \alpha)\beta\chi\rho, \quad (27)$$

$$\rho_{i+1,j+1,k+1} = \alpha\beta\chi\rho, \quad (28)$$

where

$$\alpha = \frac{x - (i + 0.5) \cdot dx'}{dx'}, \quad \beta = \frac{y - (j + 0.5) \cdot dy'}{dy'}, \quad \chi = \frac{z - (k + 0.5) \cdot dz'}{dz'}, \quad (29)$$

$$\rho = \frac{q}{dx' dy' dz'}, \quad (30)$$

and q is the charge of the moving particle. The current densities can be easily obtained by two steps. One is to multiply the charge of the particle by its velocities in three directions, and the second step is to interpolate the product to the neighbor grids. However, there is one thing to notice that the number of the adjacent nodes will change if the particles arrive at the grid boundary. In the implementation, if the distance between a particle and any boundary is less than a half grid, for instance, $x < 0.5 \cdot dx$, or $x > (i + 0.5) \cdot dx$, we will denote it as a boundary particle. When the particles stay at boundary faces or boundary edges, the charge will be allocated on 4 or 2 adjacent nodes, respectively. When it comes to the boundary corner, only the corner grid will be allocated.

The field interpolation has a reverse execution process to the charge interpolation method. The EM fields acting on a certain particle are interpolated by the weighted summation of the EM fields in the adjacent grids. Thus, the electric field on a particle in grid (i, j, k) can be evaluated as

$$\begin{aligned}
\mathbf{E}_{i,j,k}^q = & (1-\alpha)(1-\beta)(1-\chi)\mathbf{E}_{i,j,k} + \alpha(1-\beta)(1-\chi)\mathbf{E}_{i+1,j,k} \\
& + (1-\alpha)\beta(1-\chi)\mathbf{E}_{i,j+1,k} + (1-\alpha)(1-\beta)\chi\mathbf{E}_{i,j,k+1} \\
& + \alpha\beta(1-\chi)\mathbf{E}_{i+1,j+1,k} + \alpha(1-\beta)\chi\mathbf{E}_{i+1,j,k+1} \\
& + (1-\alpha)\beta\chi\mathbf{E}_{i,j+1,k+1} + \alpha\beta\chi\mathbf{E}_{i+1,j+1,k+1}
\end{aligned} \quad . \quad (31)$$

The dimensionless parameters in Eq. (31) are the same as those in Eq. (29). One can obtain the magnetic field on the particle accordingly. Note that the number of the adjacent nodes which participate in pushing the particle obeys the same rule in the particle interpolation.

3 Computational Model and Result

To verify our code JefiPIC, we invite other three 3-D codes for comparison in three models with different electron initial conditions. One is a mature PIC code UNIPIC, one is an open-source PIC code EPOCH and the other is a plasma simulator RGB-Maxwell. UNIPIC and EPOCH are the mature and traditional PIC codes based on FDTD method and the third one solves the Boltzmann equations employing the same Jefimenko's equations as in JefiPIC. The particle boundaries of the four codes are all absorbing boundaries, while the field boundaries of the difference-based codes adopt the convolutional perfect matched layers (CPML) and those of the integral equations-based codes use the natural cut-off boundary.

In JefiPIC, since the numerical values for physical quantities must be within the range of machine precision, i.e., float64, we need to convert the quantities from International Unit of System (SI) to a new unit system. In this paper, we use the Flexible Unit (FU) as in RGB-Maxwell (see appendix for a short introduction of FU). By choosing proper values for vacuum permittivity ε_0 , reduced Planck constant \hbar , speed of light c , and λ which relates the energy in SI and FU, we can limit most of the numerical values in machine precision. **Note that the use of FU does not change the physics of the plasma system.**

In the four codes, we divide the computational region with the same spatial grid size $dx = dy = dz = 10^{-5}$ m. The total computational time is 10^{-9} s. In UNIPIC and EPOCH, owing to the difference method, time step dt needs to satisfy the CFL condition [43] which limits the time step according to the grid sizes

$$c \cdot dt \leq \frac{1}{\sqrt{\frac{1}{(dx)^2} + \frac{1}{(dy)^2} + \frac{1}{(dz)^2}}} \quad . \quad (32)$$

JefiPIC and RGB-Maxwell utilize Jefimenko's equations instead, so there is little limit to the time step. However, in order to gain a more accurate result, we set the time step $dt = 10^{-13}$ s with 10^4 time steps.

Though we adopt different models, the following parameters are the same. We choose the same total computational region of size $1 \cdot dx \times 251 \cdot dy \times 111 \cdot dz$ in JefiPIC and RGB-Maxwell, and of size $3 \cdot dx \times 251 \cdot dy \times 111 \cdot dz$ in EPOCH and UNIPIC. The total initial charges of the electrons are all 5×10^{-14} C with electron number of 3.125×10^5 . In JefiPIC, each macro-particle is tracked in a CUDA kernel. Since the maximum number of CUDA kernels is around 10^9 on one A100 GPU card, we can simulate at most 10^9 particles at the same time in JefiPIC. Thus, in order to decrease the numerical noise, we use one macro-particle to stand for 1/100 electron, and as a result there are 3.125×10^7 particles in the JefiPIC simulation. In EPOCH, the code dynamically adjusts the weight of the particles so that the particle number in each grid is around 100. In UNIPIC, we need to set a proper particle weight to obtain both the acceptable numerical noise and execution time. In RGB-Maxwell, the initial condition is a distribution function defined on the six-dimensional phase space. We restrict the transverse motions of the electrons in the XOZ plane by posing a constant magnetic field $B = 10$ T along the y -direction. In our simulation, we use the eV

unit to represent the initial velocity.

3.1 Electrostatic effect is dominant

As mentioned before, the most advantageous term of the integral-based PIC method is the ability to handle the electrostatic and low-frequency EM fields. Here, we compare the evolution of a batch of electrons with no initial velocity by JefiPIC, EPOCH, and RGB-Maxwell firstly. These electrons are initially placed in a cuboid region of $1 \cdot dx \times 1 \cdot dy \times 101 \cdot dz$ with ranges from $0 \cdot dx$ to $1 \cdot dx$ ($1 \cdot dx$ to $2 \cdot dx$ in EPOCH), $124 \cdot dy$ to $125 \cdot dy$ and $5 \cdot dz$ to $106 \cdot dz$ uniformly, shown in Figure 2.

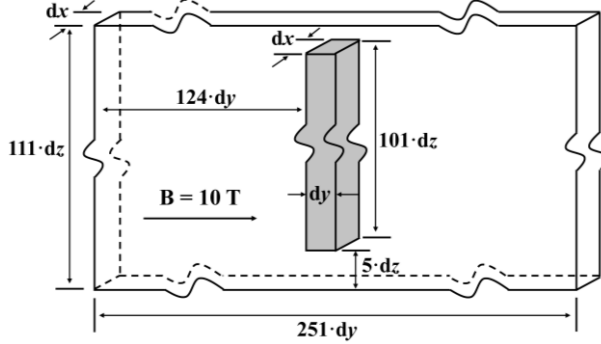
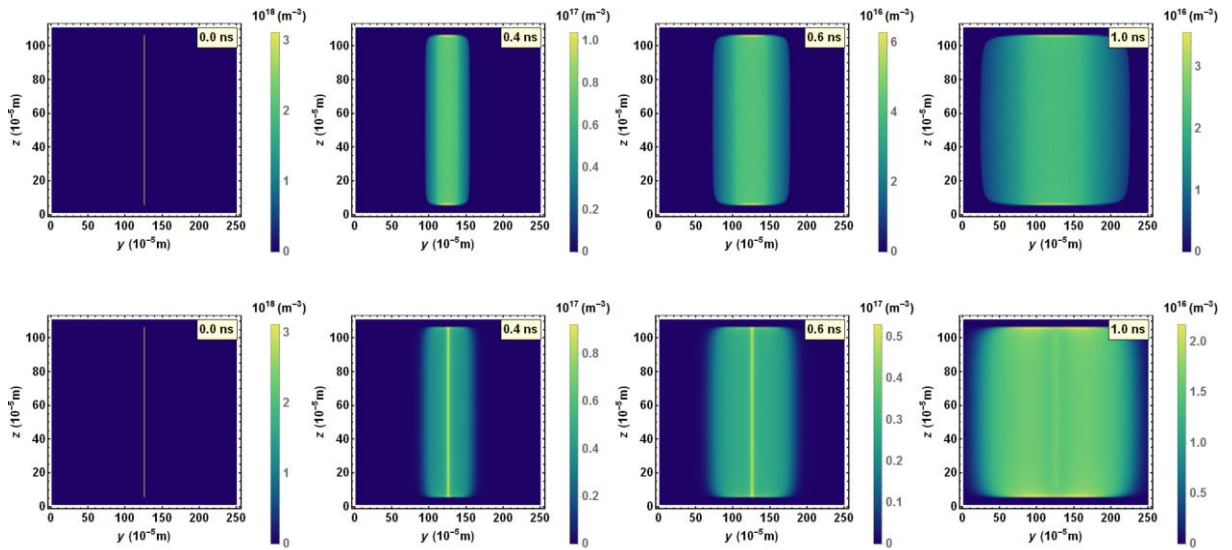


Figure 2. The initial particle distribution. The total computational region is of size $1 \cdot dx \times 251 \cdot dy \times 111 \cdot dz$ in JefiPIC and RGB-Maxwell, and of size $3 \cdot dx \times 251 \cdot dy \times 111 \cdot dz$ in EPOCH. The particles are placed in the shaded region uniformly in the cuboid volume of $1 \cdot dx \times 1 \cdot dy \times 101 \cdot dz$ with $0 \cdot dx$ to $1 \cdot dx$ ($1 \cdot dx$ to $2 \cdot dx$ in EPOCH), $124 \cdot dy$ to $125 \cdot dy$ and $5 \cdot dz$ to $106 \cdot dz$. The velocities of the particles are zero.

Due to the repulsion from one another, particles are supposed to diffuse from the center to both sides along the y axis. The particles simulated by JefiPIC and RGB-Maxwell continuously spread out as shown in Figure 3. However, EPOCH fails to exhibit the reasonable distribution with no particle diffusion at all time steps. The results are explainable that since JefiPIC and RGB-Maxwell are based on Jefimenko's equations which mimic the electric field given both the charges and currents; while the FDTD-based PIC only obtains the electric field from the current term. In this condition, once the particles have no initial velocity, no current will be generated, and thus we will obtain zero EM fields from Eqs. (1) ~ (2) in EPOCH.



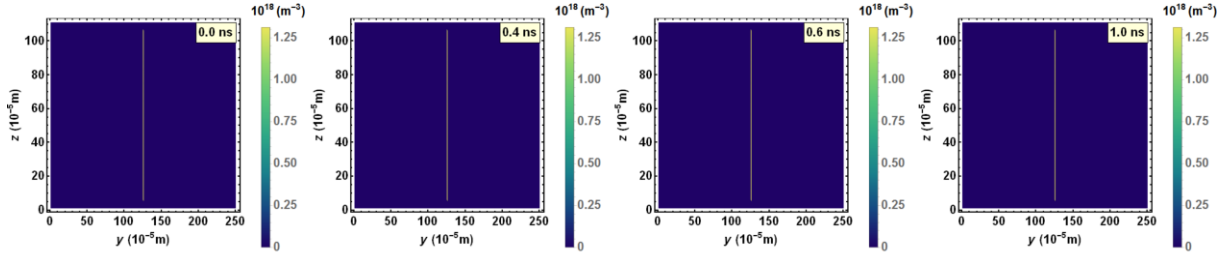


Figure 3. Particle distributions at different times a) 0.0 ns, b) 0.4 ns, c) 0.6 ns, and d) 1.0 ns. The three rows correspond to the results obtained by JefiPIC, RGB-Maxwell and EPOCH, respectively.

To further verify JefiPIC, we compare its electron number density distribution with the analytical solution [44]

$$\psi \sim \frac{1}{\tau[y^2/2\tau^2 + 1/\psi_0]} \quad (33)$$

where ψ , τ , and y are the normalized number density, time and distance. In Figure 4, we see that the particle distributions given by JefiPIC matches with the analytical solution in general. The result confirms the advantage of JefiPIC in simulating plasma systems especially when the electrostatic effect is dominant. However, the above model is a rare case in the physical world, where the charged particles more or less have some initial kinetic energy. Here, we emphasize that if the electrostatic forces are dominant, the FDTD-based PIC codes will present the unsatisfactory results. To see this, we perform another two comparisons with electron emission of mono-energy initial velocities and obeying certainty velocity spectrum.

Meanwhile, we have also provided other related simulations in the Appendix for readers to further perceive the results given by JefiPIC.

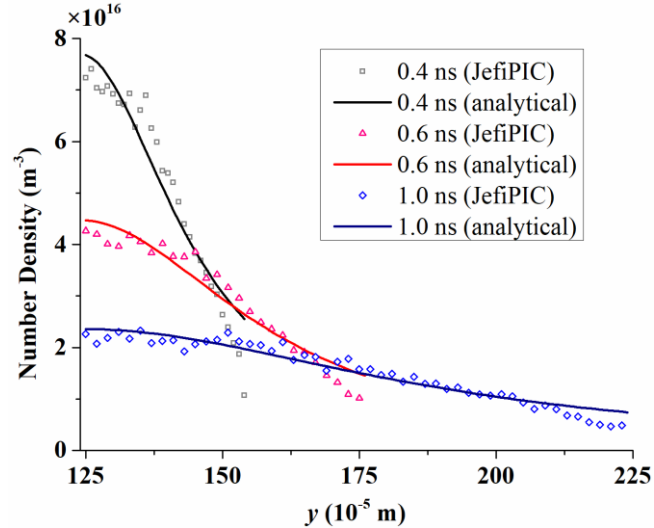


Figure 4. Simulated particle number density distribution by JefiPIC and the analytical solution from Ref [44] at $t = 0.4$ ns, 0.6 ns and 1.0 ns. The data are extracted from the grids [0-dx to 1-dx, 125-dy to 225-dy, 54-dz to 55-dz]. The gray hollow square, pink hollow triangle and blue hollow rhombus represent the results by JefiPIC, and the black, red and dark blue lines represent the analytical results.

3.2 Mono-energy electron emission

In this subsection, we work on the mono-energy electron volume-emission model and compare the results of JefiPIC with those of EPOCH and RGB-Maxwell. The electrons are initially placed in a cuboid region of $1 \cdot dx \times 1 \cdot dy \times 101 \cdot dz$ with ranges from $0 \cdot dx$ to $1 \cdot dx$ ($1 \cdot dx$ to $2 \cdot dx$ in EPOCH), $9 \cdot dy$ to $10 \cdot dy$ and

$5 \cdot dz$ to $106 \cdot dz$ uniformly, shown in Figure 5. The initial velocities of all the particles are 10 eV.

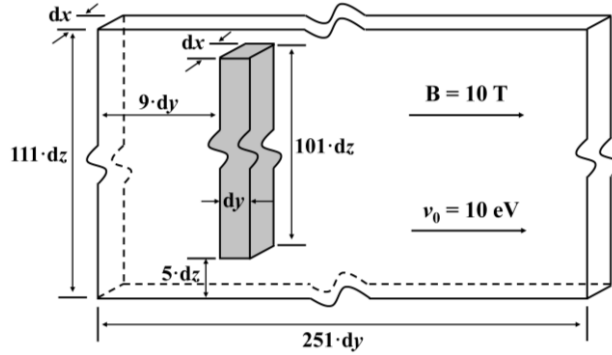


Figure 5. The initial particle distribution in the simulation. The total computational region is of size $1 \cdot dx \times 251 \cdot dy \times 111 \cdot dz$ in JefiPIC and RGB-Maxwell, and of size $3 \cdot dx \times 251 \cdot dy \times 111 \cdot dz$ in EPOCH. The particles are placed in the shaded region uniformly in the cuboid volume of $1 \cdot dx \times 1 \cdot dy \times 101 \cdot dz$ with $0 \cdot dx$ to $1 \cdot dx$ ($1 \cdot dx$ to $2 \cdot dx$ in EPOCH), $9 \cdot dy$ to $10 \cdot dy$ and $5 \cdot dz$ to $106 \cdot dz$. The velocities of the particles are 10 eV.

Figure 6 shows the particle distribution by the three codes at different time snapshots. As we can see, the general distributions are similar that the particles locate almost the same regions at each time. The particles are all repelled from each other by the electric fields in the y -direction and limited in the XOZ plane by the external magnetic field. Meanwhile, results given by JefiPIC and RGB-Maxwell are more similar since they use the same EM solver. RGB-Maxwell solves the Boltzmann equations directly, which is already the ensemble averaged result. Thus, its particle distributions are smoother compared with those of JefiPIC, in which we observe a clearer and denser layer in the central electron beam. The densest region of the particle distribution from EPOCH locates in the center region which is quite different from the other two codes, indicating that the electrostatic effect is not completely captured in EPOCH. This behavior is understandable since the FDTD-based simulation is weak at solving the electrostatic problems, which is revealed in Sec. 3.1. Meanwhile, we have also observed undesired edge effects from EPOCH. The severe edge effects are mainly caused by the invented positive charge/fields and particle interpolation method.

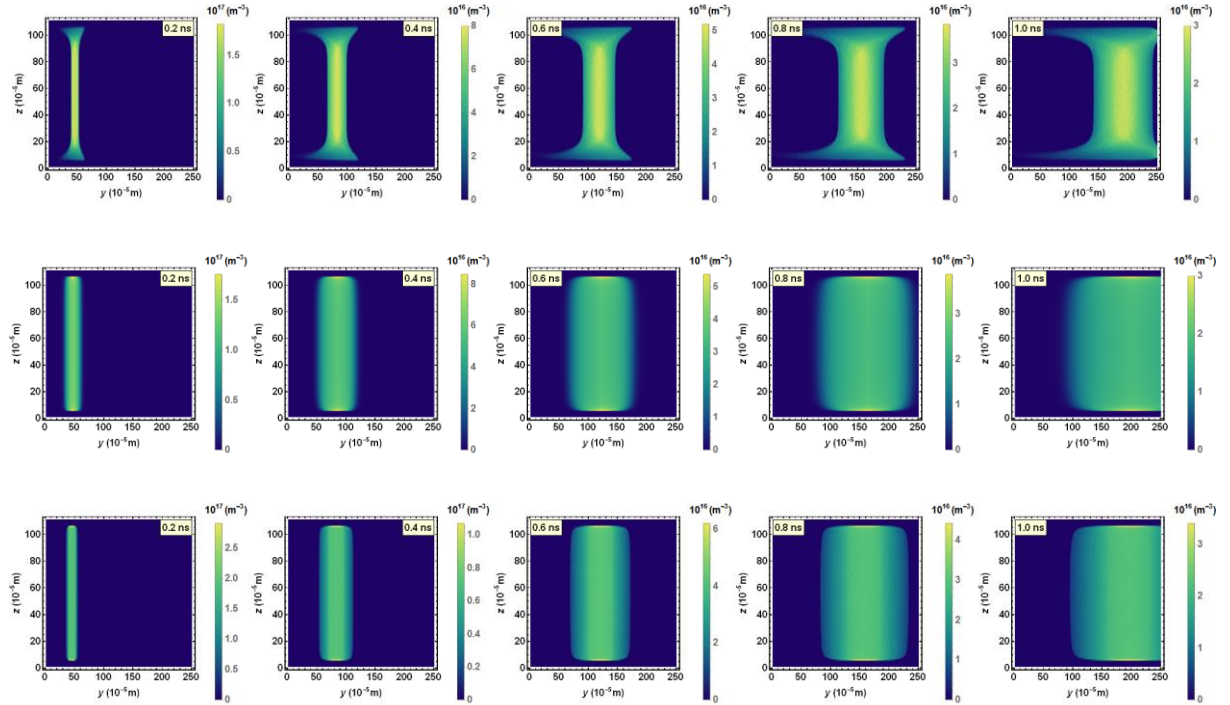


Figure 6. Particle distribution in the YOZ plane. The three rows correspond to the results from EPOCH, RBG-Maxwell and JefiPIC. The

time snapshots are chosen to be $t = 0.2, 0.4, 0.6, 0.8$ and 1.0 ns.

To further perceive that EPOCH does not capture the full effect of the electric fields, we give the electron number density along y -axis (here, we choose $i = 1, k = 55$ in EPOCH and $i = 0, k = 55$ in the other two codes) at different times in Figure 7. With a higher-order charge interpolation method, EPOCH allocates the electrons to the adjacent grids, and its initial number density is less than those of the other two (Figure 7 (a)). As the time passes by, EPOCH gives denser charged particles in the center of the electron beam and more dilute at the edges (Figure 7 (b) and (c)), though the total charge is conserved all the time.

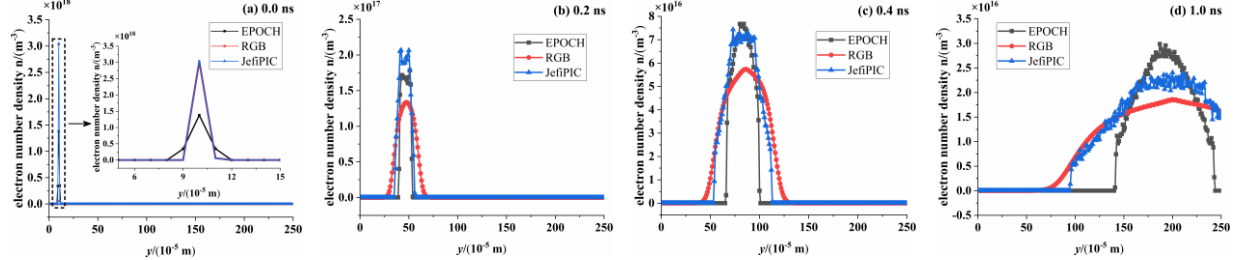


Figure 7. The electron number density along y -axis. The grid indices in the x and z -axes are $i = 1, k = 55$ in EPOCH and $i = 0, k = 55$ in the other two codes. The black squares, red circles and blue triangles indicate the result from EPOCH, RGB-Maxwell and JefiPIC.

From Figure 7, it should be anticipated that the peak of the electric fields from EPOCH will be higher than the other two when EPOCH gives the highest density peak. In Figure 8, we plot the electric fields at two diagnosing points ($i = 1, j = 50, k = 55$) and ($i = 1, j = 80, k = 55$) in EPOCH and ($i = 0, j = 50, k = 55$) and ($i = 0, j = 80, k = 55$) in RGB-Maxwell and JefiPIC. Generally, we see that JefiPIC and RGB-Maxwell give the similar waveforms of the electric fields with the same EM solver. However, we do not get the highest peak by EPOCH as expected. On the contrary, the larger electron density gives the lowest electric field peak value. The counterintuitive phenomenon shows that EPOCH lacks the ability to fully mimic the electrostatic or low-frequency fields. Meanwhile, the electric field pulse given by EPOCH has a smaller width, which indicates that the electric fields are only produced when the particles pass by the diagnosing point. The results are reasonable since FDTD updates the EM fields according to the local sources, and the EM fields generated by far regions may be distorted. However, we emphasize that the arrival time of the electric peak of the three codes almost coincide with one another, indicating that the particle motions are similar.

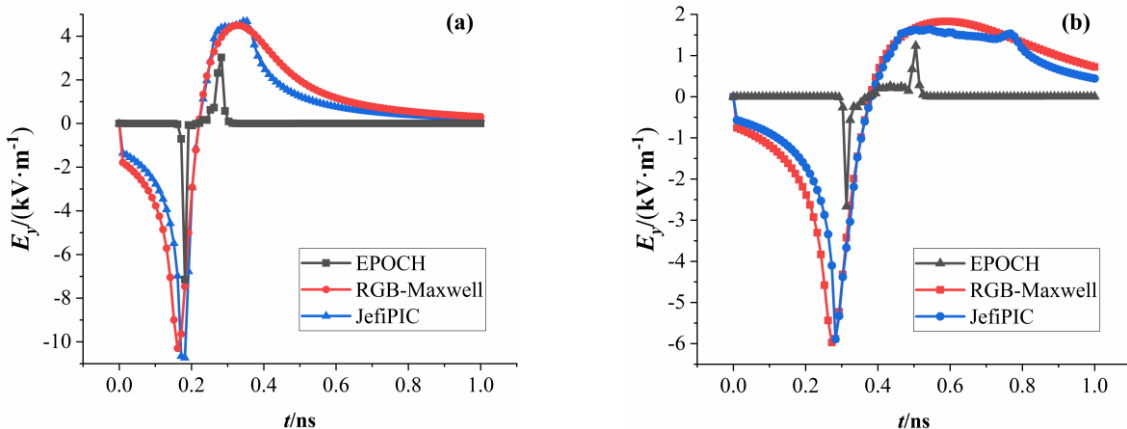


Figure 8. The electric fields a) at point ($i = 1, j = 50, k = 55$) by EPOCH and point ($i = 0, j = 50, k = 55$) by RGB-Maxwell and JefiPIC, and b) at point ($i = 1, j = 80, k = 55$) by EPOCH and point ($i = 0, j = 80, k = 55$) by RGB-Maxwell and JefiPIC. The black squares, red circles and blue triangles indicate the result from EPOCH, RGB-Maxwell and JefiPIC.

As mentioned above, by using GPU, the execution time of JefiPIC is acceptable, which is of the same order as and even shorter than the others. The detailed calculation information is shown in Table 1. In EPOCH, one needs to set the time step dt very small to satisfy the CFL condition, while in JefiPIC this constraint is not required. Therefore, we see that JefiPIC is faster than EPOCH in the current condition.

Table 1. The computational time of EPOCH, RGB-Maxwell and JefiPIC

Code	EPOCH	RGB-Maxwell	JefiPIC
Time cost	~1 h	~ 0.8 h	~0.6 h
Device info	Intel Xeon Gold 6132	Tesla A100	Tesla A100

Meanwhile, we also test the time consumption of JefiPIC with the increase of the macro-particle numbers to provide readers with further reference. It can be seen from Figure 9 that if the particle number is less than one percent of the limitation of CUDA kernel (~ a bit less than 10^7), the computational time keeps short and changes little. This is due to the high degree of parallelism on GPU and less data transferring between CPU and GPU. However, once the particle number is beyond 10^7 , the time cost will be multiplying. Note that the allocated kernel number (i.e., the particle number in JefiPIC) must not exceed the limitation by CUDA (~ 10^9) or the computation will fail. Fortunately, 10^7 ~ 10^8 macro-particles are quite enough for the usual simulation within the controlled noises.

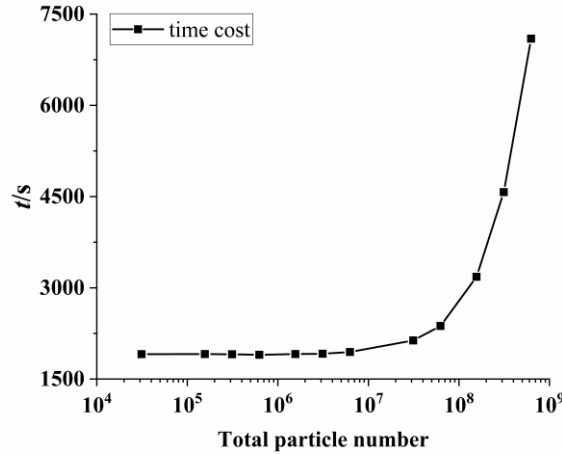


Figure 9. The time cost of JefiPIC with different particle numbers. Enslaved to the CUDA kernel, the upper limit of the particle number is around 10^9 .

3.3 Electron emission obeying certain velocity spectrum

In this subsection, we choose another FDTD-based PIC code UNIPIC to further demonstrate the advantage of the integral-based PIC codes in solving electrostatic problems. In this model, the electrons are emitted from the shaded face, shown in Figure 10. The initial velocities are only in the y -direction randomly from 0 eV to 10 eV.

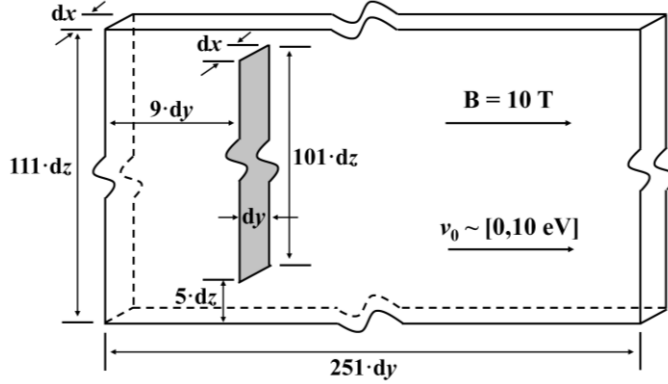


Figure 10. The initial electron distribution in the simulation. The total computational region is of size $1 \cdot dx \times 251 \cdot dy \times 111 \cdot dz$ in JefiPIC, and of size $3 \cdot dx \times 251 \cdot dy \times 111 \cdot dz$ in UNIPIC. The particles are placed uniformly on the shaded rectangle face of $y = 9 \cdot dy$ and $1 \cdot dx \times 101 \cdot dz$ with $0 \cdot dx$ to $1 \cdot dx$ ($1 \cdot dx$ to $2 \cdot dx$ in UNIPIC) and $5 \cdot dz$ to $106 \cdot dz$. The velocities of the particles obey random distribution from 0 eV to 10 eV.

The calculated particle distributions from JefiPIC and UNIPIC are presented in Figure 11 at two snapshots. It is obvious that the two series of particles are overall similar, which verifies the results of our code to a certain extent. Besides, we also find that the particles from JefiPIC spread a larger region than from UNIPIC. Table 2 lists the maximum y -direction displacement and velocity of the particles at the corresponding times. It is shown that the particles simulated by JefiPIC have larger velocities and thus moving further than those from UNIPIC. The difference in the particle distributions is caused by the difference of Coulomb forces induced by themselves, suggesting that UNIPIC does not capture the full electric effects.

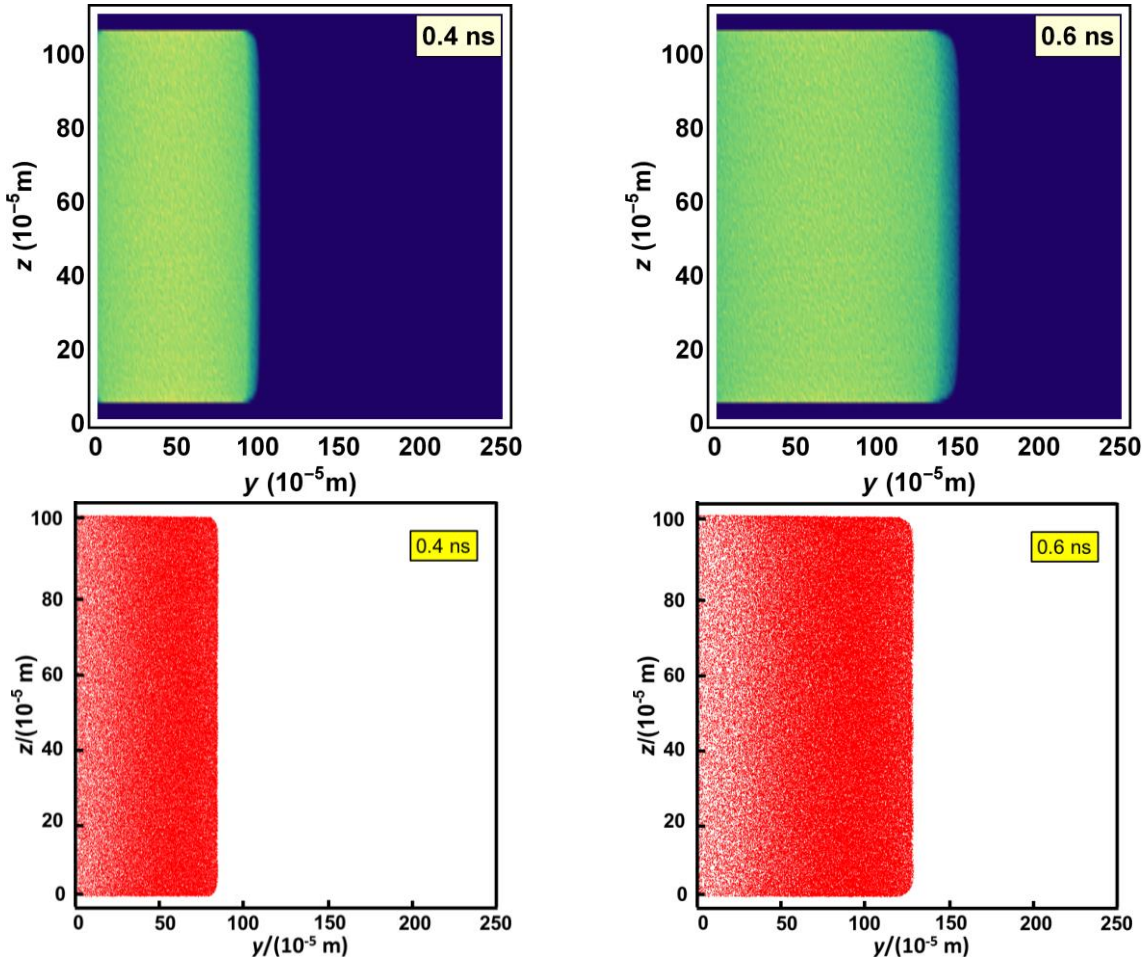


Figure 11. Particle distribution from (a) JefiPIC and (b) UNIPIC at $t = 0.4$ ns and $t = 0.6$ ns with initial velocities only in the y -direction randomly from 0 eV to 10 eV.

Table 2. Comparison of the maximum particle displacement and velocity between JefiPIC and UNIPIC

Time/ns	Maximum Displacement/m		Maximum Velocity/(m·s ⁻¹)	
	JefiPIC	UNIPIC	JefiPIC	UNIPIC
0.4	1.01×10^{-3}	8.49×10^{-4}	2.47×10^6	2.26×10^6
0.6	1.51×10^{-3}	1.30×10^{-3}	2.53×10^6	2.30×10^6

Meanwhile, the electrostatic field is the dominant factor in the interactions among the moving charged particles, and the integral method naturally has the advantage over the difference method to deal with it. To see this, we exhibit the y -direction electric fields at point ($i = 0, j = 50, k = 55$) in JefiPIC and at point ($i = 1, j = 50, k = 55$) in UNIPIC in Figure 12. The differences between the two electric fields lies in three aspects: a) the field peak time by JefiPIC is earlier, b) the width of the field pulse by JefiPIC is larger, and c) the field peak by JefiPIC is partly larger. Hence, the fields given by the integral equations can accelerate the particles more prominently in a longer time, which leads to the larger particle distribution and the earlier peak time of electric fields.

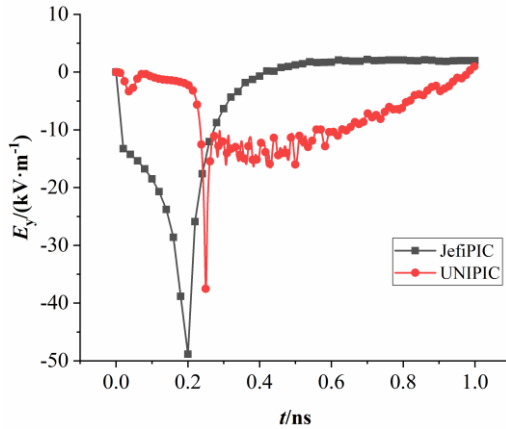


Figure 12 The y -direction electric field at point ($i = 0, j = 50, k = 55$) derived from JefiPIC and at point ($i = 1, j = 50, k = 55$) from UNIPIC. The black square and red circle represent the result from JefiPIC and UNIPIC.

In addition, we also compare the time performance of each code. Under this condition, UNIPIC is operated on CPU with Intel Xeon Processor E7450 through 200 threads and the calculation takes over 6 hours, while JefiPIC finishes the work within only 0.5 hour on one GPU A100 card.

4 Discussion and Conclusion

In this paper, we have proposed a plasma simulation package JefiPIC, which solves the challenging task of describing plasma systems in terms of a 3-D particle-in-cell method combined with the Jefimenko's equations on GPU. The particles are pushed by the traditional particle simulation method, and the volume-weighted charge and field interpolation methods are employed. Because the locations to allocate fields, charge density and current density are changed from the FDTD to Jefimenko's equations, we have modified the interpolation method accordingly. Through the comparisons with the results from UNIPIC, EPOCH and RGB-Maxwell, we verify the credibility of JefiPIC. It can be seen as a consistent combination of the FDTD-based electromagnetic PIC and time-retarded electrostatic Poisson PIC. Our first-order accurate PIC code has the similar results as the second-order accurate Boltzmann equations, and shows a

better solution of the electrostatic problem compared with results solved by the difference equations.

Meanwhile, the time cost of JefiPIC is acceptable in dealing with the plasma problem with open boundary conditions. Though, the current version of JefiPIC only solves the collisionless Vlasov equations, the interactions between electrons and neutral molecules or charged ions are going be added to make the code more widely applicable.

Acknowledgement

We thank Prof. J. Wang for the helpful discussions on the PIC simulations. The work is supported by the National Natural Science Foundation of China (NSFC) under Grants No. 12105227.

Reference

- [1]. J. Dawson, One-dimensional plasma model, *The Physics of Fluids*, 5(4) (Apr.1962) pp. 445-459 doi: 10.1063/1.1706638.
- [2]. A. B. Langdon and C. K. Birdsall, Theory of plasma simulation using finite-size particles, *The Physics of Fluids*, 13(8) (Aug. 1970) pp. 2115-2122 doi: 10.1063/1.1693209.
- [3]. C. K. Birdsall and D. Fuss, Clods-in-clouds, clouds-in-cells physics for many-body plasma simulation, *Journal of Computational Physics*, 3(4) (Apr. 1969) pp. 494-511, doi: 10.1016/0021-9991(69)90058-8.
- [4]. B. Marder, A method for incorporating Gauss' law into electromagnetic PIC codes, *Journal of Computational Physics*, 68(1) (Jan. 1987) pp. 48-55 doi: /10.1016/0021-9991(87)90043-X.
- [5]. J. Villasenor, O. Buneman, Rigorous charge conservation for local electromagnetic field solvers, *Computer Physics Communications*, 69(2-3) (Mar.-Apr. 1992) pp. 306-316 doi: 10.1016/0010-4655(92)90169-Y.
- [6]. C. K. Birdsall, Particle-in-cell charged-particle simulations, plus Monte Carlo collisions with neutral atoms, PIC-MCC, *IEEE Transactions on Plasma Science*, 19(2) (Apr. 1991) pp. 65-85 doi: 10.1109/27.106800.
- [7]. V. Vahedi, M. Surendra, A Monte Carlo collision model for the particle-in-cell method: applications to argon and oxygen discharges, *Computer Physics Communications*, 87(1-2) (May 1995) pp. 179-198 doi: 10.1016/0010-4655(94)00171-W.
- [8]. B. Wang, et al., Modern gyrokinetic particle-in-cell simulation of fusion plasmas on top supercomputers, *The International Journal of High Performance Computing Applications*, 33(1) (Jan. 2019) pp. 168-188 doi: 10.1177/11094342017712059.
- [9]. T. D. Arber, et al., Contemporary particle-in-cell approach to laser-plasma modelling, *Plasma Physics and Controlled Fusion*, 57(11) Article. 113001 (Sept. 2015) doi: 10.1088/0741-3335/57/11/113001.
- [10].J. Chen and J Zhang, Impact of geometrical parameters on SGEMP responses in cylinder model, *Nuclear Engineering and Technology*, 54(9) (Sept., 2022) pp. 3415-3421 doi: 10.1016/j.net.2022.04.018.
- [11].H. Zhang, et al. Particle-in-cell simulations of low-pressure air plasma generated by pulsed x rays, *Journal of Applied Physics*, 130(17) Article. 173303 (Nov. 2021) doi:10.1063/5.0057841.
- [12].Z. Xu, et al., A code verification for the cavity SGEMP simulation code LASER-SGEMP, *IEEE Transactions on Nuclear Science*, 68(6) (Jun. 2021) pp. 1251-1257 doi: 10.1109/TNS.2021.3078739.
- [13].Q. Lu, et al., Particle-in-cell simulations of whistler waves excited by an electron K distribution in space plasma, *Journal of Geophysical Research Space Physics*, 115 Article. A02213 (Feb. 2010) doi: 10.1029/2009JA014580.
- [14].J. Chen, et al., 2D planar PIC simulation of space charge limited current with geometrical parameters, varying temporal-profile and initial velocities, *IEEE ACCESS*, 10 (2022) pp. 28499-28508 doi: 10.1109/ACCESS.2022.3158747.
- [15].J. Wang, A megawatt-level surface wave oscillator in Y-band with larger oversized structure driven by

annular relativistic electron beam, *Scientific Reports*, 8 Article. 6978 (May 2018) doi: 10.1038/s41598-018-25466-w

[16].D. R. Welch, Fast hybrid particle-in-cell technique for pulsed-power accelerators, *Physical review accelerators and beams*, 23(11) Article. 110401 (Nov. 2020) doi: 10.1103/PhysResAccelBeam.23.110401.

[17].B. Goplen, et al., User-configurable MAGIC for electromagnetic PIC calculations, *Computer Physics Communications*, 87(1-2) (May 1995) pp. 54-86 doi: 10.1016/0010-4655(95)00010-D.

[18].J. P. Verboncoeur, et al., An object-oriented electromagnetic PIC code, *Computer Physics Communications*, 87(1-2) (May 1995) pp. 199-211 doi: 10.1016/0010-4655(94)00173-Y.

[19].J. D. Blahovec, et al., 3-D ICEPIC simulations of the relativistic klystron oscillator, *IEEE Transactions on Plasma Science*, 28(3) (June 2000) pp. 821-829 doi: 10.1109/27.887733.

[20].J. Wang, et al., UNIPIC code for simulations of high power microwave devices, *Phys. Plasmas*, 16(3) (Mar. 2009) Article. 033108 doi:10.1063/1.3091931.

[21].T. D. Arber, et al., Contemporary particle-in-cell approach to laser-plasma modelling, *Plasma Physics and Controlled Fusion*, 57(11) Article. 113001 (Sept. 2015) doi: 10.1088/0741-3335/57/11/113001.

[22].C. P. Ridgers, et al., Modelling gamma-ray photon emission and pair production in high-intensity laser-matter interactions, *Journal of Computational Physics*, 260(1) (Mar. 2014) pp. 273-285 doi: 10.1016/j.jcp.2013.12.007.

[23].K. Yee, Numerical solution of initial boundary value problems involving maxwell's equations in isotropic media, *IEEE Transactions on Antennas and Propagation*, 14(3) (May 1966) pp. 302-307 doi: 10.1109/TAP.1966.1138693.

[24].D-Y. Na, Y. A. Omelchenko, H. Moon, B. V. Borges, F. L. Teixeira, Axisymmetric Charge-Conservative Electromagnetic Particle Simulation Algorithm on Unstructured Grids: Application to Microwave Vacuum Electronic Devices, *Journal of Computational Physics*, 346 (Oct. 2017) pp. 295-317 doi: 10.1016/j.jcp.2017.06.016.

[25].D-Y. Na, H. Moon, Y. A. Omelchenko, and F. L. Teixeira, Relativistic extension of a charge-conservative finite element solver for time-dependent Maxwell-Vlasov equations, *Physics of Plasmas*, 25(1) Article. 013109 (Jan. 2018) doi: 10.1063/1.5004557.

[26].J. P. Verboncoeur, Symmetric Spline Weighting for Charge and Current Density in Particle Simulation, *Journal of Computational Physics*, 174(1) (Nov. 2001) pp. 421-427 doi: 10.1006/jcph.2001.6923.

[27].T. Zh. Esirkepov, Exact charge conservation scheme for Particle-in-Cell simulation with an arbitrary form-factor, *Computer Physics Communications*, 135(2) (Apr. 2001) pp. 144-153 doi: 10.1016/S0010-4655(00)00228-9.

[28].Y. Wang, et al., Charge conserving emission technique for three-dimensional conform particle-in-cell simulations, *High Power Laser and Particle Beams*, 28(3) (Mar. 2016) Article. 033020 doi: 10.11884/HPLPB201628.033020.

[29].O. D. Jefimenko, Electricity and magnetism: an introduction to the theory of electric and magnetic fields, Electret Scientific Co, Star City, W. Va, 1989.

[30].D. Griffiths, Introduction to electrodynamics, Prentice Hall, Upper Saddle River, N.J, 1999.

[31].G. G. Howes, Laboratory space physics: Investigating the physics of space plasmas in the laboratory, 25(5) (Apr. 2018) Article. 055501 doi: 10.1063/1.5025421.

[32].J. Zhang, et al., Charge-dependent directed flows in heavy-ion collisions by Boltzmann-Maxwell equations, *Physical Review Research*, 4(3) (Aug. 2022) Article. 033138 doi: 10.1103/PhysRevResearch.4.033138.

[33].G. Peng, et al., Two typical collective behaviors of the heavy ions expanding in cold plasma with ambient magnetic field, *Physics of Fluids*, 33 Article. 076602 (Jul. 2021) doi: 10.1063/5.0053404

[34].S. H. Brecht and D. J. Larson, The physics of ion decoupling in magnetized plasma expansions,

Journal of Geophysical Research: Space Physics, 116(A11) Article. A11310 (Nov. 2011) doi: 10.1029/2011JA016904.

[35].J. Chen, et al., Simulation of SGEMP using particle-in-cell method based on conformal technique, IEEE Transactions on Nuclear Science, 66(5) (May, 2019) pp. 820-826 doi:10.1109/TNS.2019.2911933.

[36].M. Gaffar and D. Jiao, On the low-frequency breakdown of FDTD, 2015 IEEE International Symposium on Antennas and Propagation & USNC/URSI National Radio Science Meeting, (2015) pp. 338-339 doi: 10.1109/APS.2015.7304555.

[37].K. Chen, et al., New Mixed SETD and FETD methods to overcome the low-frequency breakdown problems by tree-cotree splitting, IEEE Transactions on Microwave Theory and Techniques, 68(8) (Aug. 2020) pp. 3219-3228 doi: 10.1109/TMTT.2020.2995721.

[38].J. Berenger, A perfectly matched layer for the absorption of electromagnetic waves, Journal of Computational Physics, 114(2) (Oct. 1994) pp. 185-200 doi: 10.1006/jcph.1994.1159.

[39].G. Mur, Absorbing boundary conditions for the finite-difference approximation of the time-domain electromagnetic-field equations, IEEE Transactions on Electromagnetic Compatibility, EMC-23(4) (Nov. 1981) pp. 377-382 doi: 10.1109/TEMC.1981.303970.

[40].J. Zhang, et al., JefiGPU: Jefimenko's equations on GPU, Computer Physics Communications, 276 Article. 108328 (Jul. 2022) doi: 10.1016/j.cpc.2022.108328.

[41].H. Wu, et al., ZMCintegral: A package for multi-dimensional Monte Carlo integration on multi-GPUs, Computer Physics Communications, 248 Article. 106962 (Mar. 2020) doi: 10.1016/j.cpc.2019.106962.

[42].J. Zhang, et al., Towards a full solution of the relativistic Boltzmann equation for quark-gluon matter on GPUs, Physical Review D, 102(7) (Oct. 2020) Article. 074011 doi: 10.1103/PhysRevD.102.074011.

[43].R. Courant, K. Friedrichs and H. Lewy, On the partial difference equations of mathematical physics, IBM Journal of Research and Development, 11(2) (Mar. 1967) pp. 215-234 doi: 10.1147/rd.112.0215.

[44].K.E. Lonngren, Expansion of an electron cloud, Physical Letters A, 59(4) (Dec. 1976) pp. 285-286 doi: 10.1016/0375-9601(76)90794-5

Appendix

A. The unit conversion table

Table 3. The transform of the physical quantities from SI Unit to Flexible Unit

Physical quantity	SI Unit	Flexible Unit
Magnetic field	T	$5.01398 \times 10^{-36} / (\lambda^2 \hbar^3/2 \epsilon_0^{1/2} c^{5/2}) E^2$
Length	m	$3.16304 \times 10^{25} \hbar c \lambda E^{-1}$
Time	s	$9.48253 \times 10^{33} \hbar \lambda E^{-1}$
Electric charge	C	$1.89032 \times 10^{18} (\hbar \epsilon_0 c)^{1/2}$
Momentum	$\text{kg} \cdot \text{m} \cdot \text{s}^{-1}$	$2.99792 \times 10^8 / (c \lambda) E$
Energy	J	$1/\lambda E$
Mass	kg	$8.89752 \times 10^8 / (c^2 \lambda) E$
Electric current	A	$1.99347 \times 10^{-16} (\epsilon_0 c / \hbar)^{1/2} / \lambda E$
Electric field	$\text{V} \cdot \text{m}^{-1}$	$1.67249 \times 10^{-44} / (\lambda^2 \hbar^3/2 \epsilon_0^{1/2} c^{3/2}) E^2$
Force	$\text{kg} \cdot \text{m} \cdot \text{s}^{-2}$	$3.16153 \times 10^{-26} / (\hbar \epsilon_0 c) E^2$
Unit charge	1	$0.30286 (\hbar \epsilon_0 c)^{1/2}$

In Flexible Unit (FU), all physical quantities have the dimension of energy E. One needs to **choose proper values for λ , c , \hbar , ϵ_0 so that all numerical quantities are in the range of float64 on GPU**, where c , \hbar , ϵ_0 denote the speed of light, the reduced Planck constant, and the vacuum permittivity. λ is constant relating the energy quantity between SI and FU.

B. Verification of JefiPIC

Here we present some results obtained by JefiPIC to further comprehend how the electric field act on the particles and how much the electrostatic fields occupy in the interactions.

B.1 Change of the emission current

Firstly, we verify whether the change of the emission current will bring an obvious change or not. Here, we remain the charge density unchanged and only alter the size of the grids and the initial velocity of the electrons. The current changes with the velocity proportionally. For convenience, the energy of **10 eV** is labeled as v_0 , and the grid size of **10⁻⁵ m** is labeled as dx . Then, we choose other three velocities and grid sizes for comparison, namely: a) $0.01 \cdot v_0$ and $0.01 \cdot dx$, b) $0.1 \cdot v_0$ and $0.1 \cdot dx$, and c) $10 \cdot v_0$ and $10 \cdot dx$, and the total charge changes accordingly.

The four groups of particle distributions and electric fields at point ($i = 0, j = 50, k = 55$) are displayed in Figure 13 and Figure 14, respectively. It is observed that if we change the particle velocities and grid sizes with the same order of magnitude, the waveforms of the electric fields are almost the same with different magnitudes. The result is reasonable since the particle densities are the same in all cases. From the first term of the right hand of Eq. (9), we know that the electrostatic field is proportional to the distance between the source and the observation point. Thus, the electric field strength and the particle repulsion scale are only proportional to that distance.

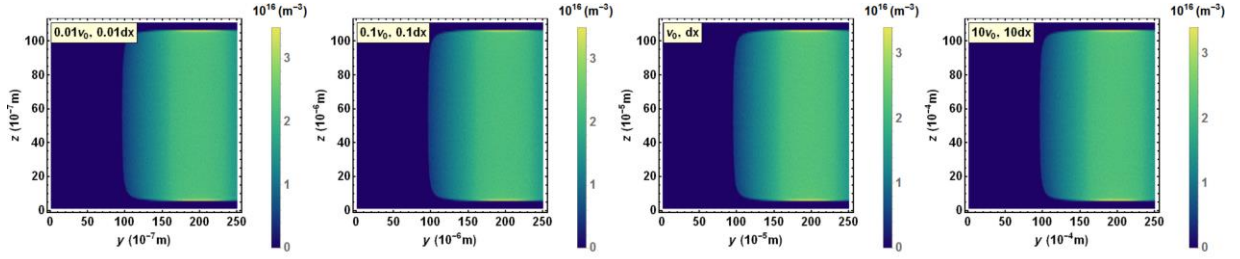


Figure 13. The particle distributions with different initial velocities and grid sizes derived from JefiPIC. The velocities and grid sizes are set as a) $0.01 \cdot v_0$ and $0.01 \cdot dx$, b) $0.1 \cdot v_0$ and $0.1 \cdot dx$, c) v_0 and dx and d) $10 \cdot v_0$ and $10 \cdot dx$.

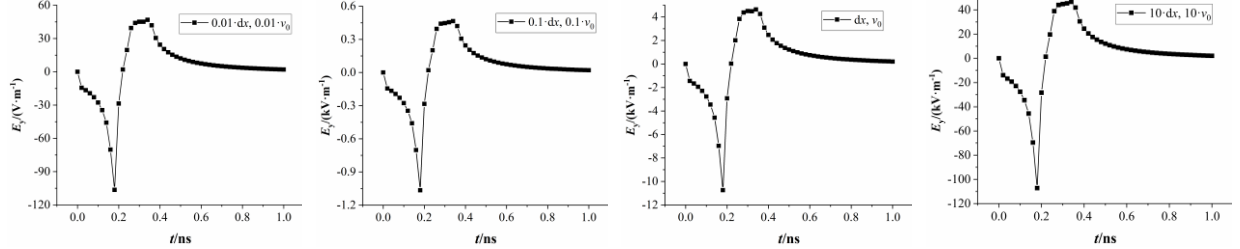


Figure 14. The electric fields at point $(i = 0, j = 50, k = 55)$ with different initial velocities and grid sizes derived from JefiPIC. The velocities and grid sizes are set as a) $0.01 \cdot v_0$ and $0.01 \cdot dx$, b) $0.1 \cdot v_0$ and $0.1 \cdot dx$, c) $1.0 \cdot v_0$ and $1.0 \cdot dx$ and d) $10 \cdot v_0$ and $10 \cdot dx$.

B.2 Change of the charge density

In this model, we change the initial charge density while keep the emission velocity v_0 the same. Figure 15 shows the particle distribution at $t = 1.0$ ns for six different cases. It is apparent that the particles spread more quickly with larger initial charge density. Figure 16 exhibits the electric fields at point $(i = 0, j = 50, k = 55)$. The time tick of the first peak arrives earlier when the initial charge density is larger, indicating that the stronger repulsion propels the particles more prominently. However, with the continuous increase of the electron density, the strong repulsion makes the second peak value smaller and the peak time delayed on the contrary. The phenomenon is rational since the particles will be more dilute at later times if the initial densities are larger.

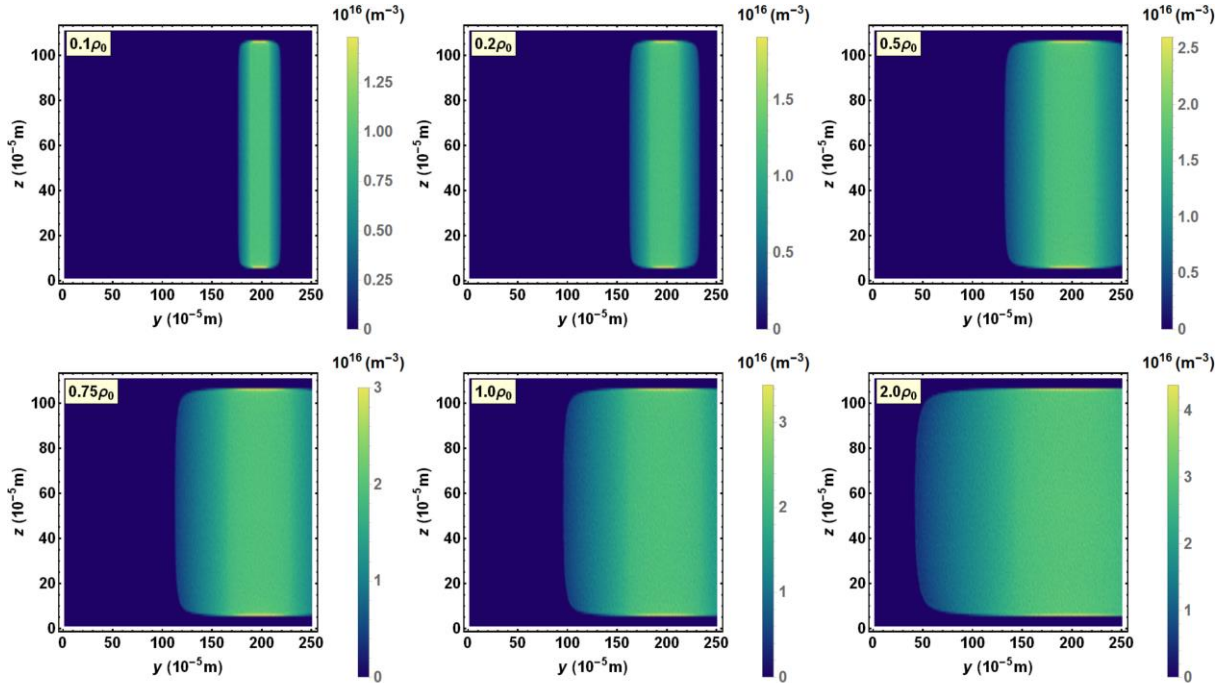


Figure 15. The particle distributions with different initial charge densities obtained from JefiPIC at $t = 1.0$ ns. The charge densities are set

as a) $0.1 \cdot \rho_0$, b) $0.2 \cdot \rho_0$, c) $0.5 \cdot \rho_0$, d) $0.75 \cdot \rho_0$, e) $1.0 \cdot \rho_0$, and f) $2.0 \cdot \rho_0$.

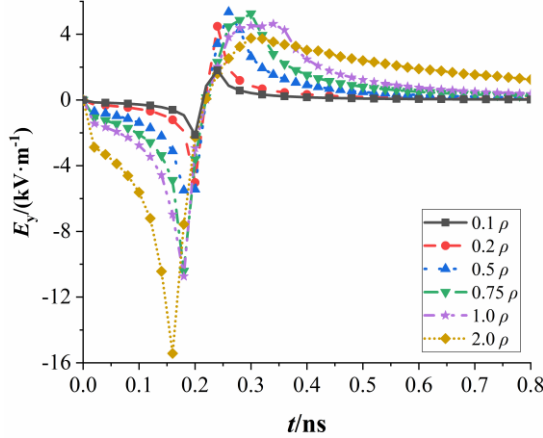


Figure 16. The electric fields at point ($i = 0, j = 50, k = 55$) with different initial charge densities from JefiPIC. Different symbols represent different charge densities.

B.3 Change of the charge density and the initial velocity

Here, we keep the electric currents the same for all cases while change the charge densities and the initial velocities. Figure 17 shows the particle distributions at $t = 0.2$ ns. We see that with the decrease of the electron density, though the emission currents are the same, the diffusion of the particle beam decreases. Thus, we confirm that the electrostatic forces are the key factors determines the electromagnetic interactions.

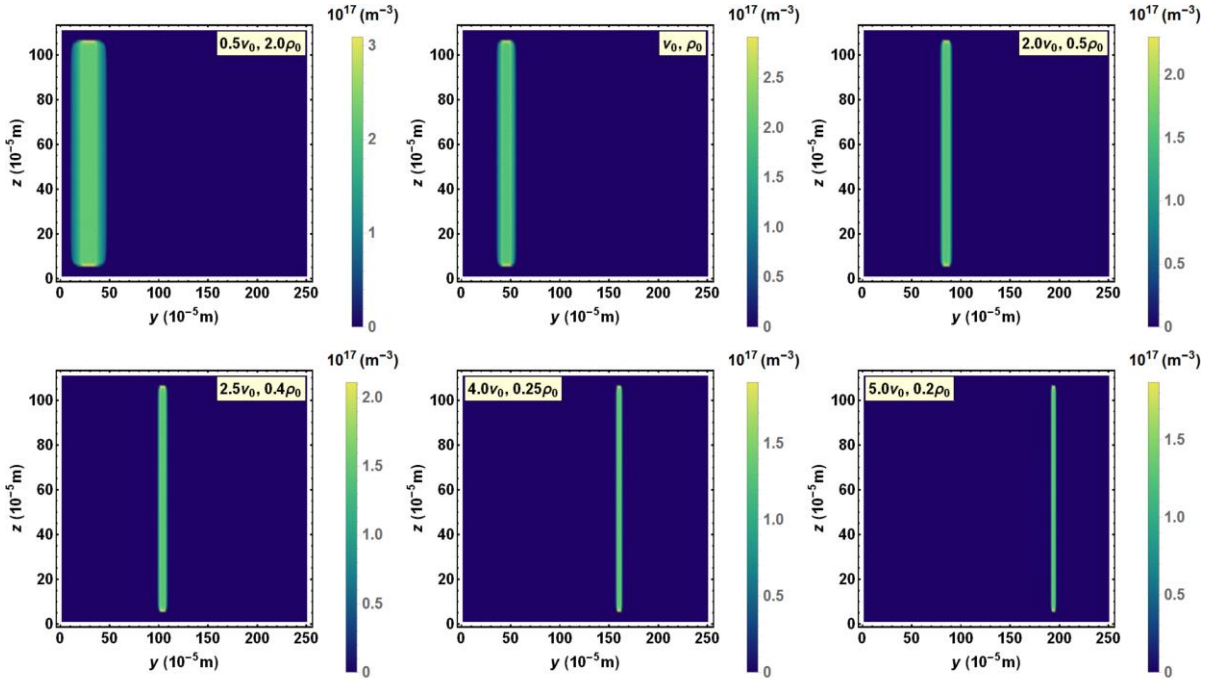


Figure 17. Particle distributions at the same time $t = 0.2$ ns with different initial particle velocities and densities, namely a) $0.5v_0, 2.0\rho_0$, b) $1.0v_0, 1.0\rho_0$, c) $2.0v_0, 0.5\rho_0$, d) $2.5v_0, 0.4\rho_0$, e) $4.0v_0, 0.25\rho_0$, and f) $5.0v_0, 0.2\rho_0$.

Figure 18 displays the latter 5 electric fields in Figure 17 at point ($i = 0, j = 50, k = 55$). As we can see, the electric field strength increases with the electron density until beyond $0.5\rho_0$. The densest electron density produces the smaller electric fields for the stronger repulsion among the particles, making the particle distribution more dilute.

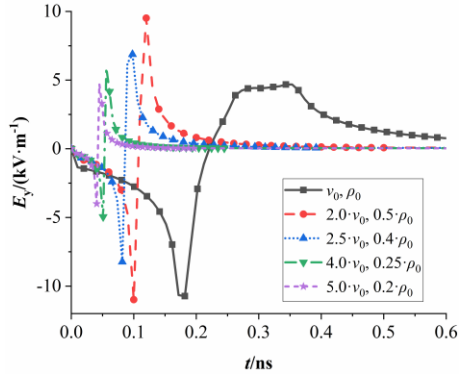


Figure 18. The electric fields at point ($i = 0, j = 50, k = 55$) with the same current but different initial charge densities and different velocities derived from JefiPIC. Different symbols represent different initial conditions.